ISSN (Print) 1226-1750
ISSN (Online) 2233-6656
Journal of Magnetics 24(2), 246-253 (2019) https://doi.org/10.4283/JMAG.2019.24.2.246

Research on the Axial Magnetic Levitation Force Acting on the Ring Magnet Suspended in Magnetic Fluid: Considering a Radial Eccentricity

Jun Yu[1,2]*, Decai Li[1,3]*, Nannan Di[1,2], and Ningning Guo[4]

[1]*School of Mechanical, Electronic and Control Engineering, Beijing Jiaotong University, Beijing 100044, China*
[2]*Key Laboratory of Vehicle Advanced Manufacturing, Measuring and Control Technology (Beijing Jiaotong University), Ministry of Education, Beijing 100044, China*
[3]*State Key Laboratory of Tribology, Tsinghua University, Beijing 100084, China*
[4]*School of Mechanical and Material Engineering, North China University of Technology, Beijing 100144, China*

(Received 11 July 2018, Received in final form 12 April 2019, Accepted 12 April 2019)

The self-suspension of magnet in magnetic fluid has been widely used in micromechanical systems, sensors, and dampers. The magnetic field associated with the ring magnet is obtained by numerical calculation and simulation through which the axial magnetic levitation force is calculated, and the numerical calculation, simulation, and experimental results agree with each other. The influence of the radial eccentricity of the ring magnet on the axial magnetic levitation force is studied, the ring magnet will experience a maximum axial magnetic levitation force without radial eccentricity. With the increase of radial eccentricity and the decrease of the distance between the bottom of the ring magnet and container, the axial magnetic levitation force will continue to decrease. But it is worth noting that the magnitude of the change caused by radial eccentricity is negligible compared to that of the axial magnetic levitation force.

Keywords : magnetic fluid levitation force, self-suspension buoyancy, ring permanent magnet, radial eccentricity

1. Introduction

The ferrofluid or magnetic fluid, a new type of functional material with fluidity and magnetism, was synthesized successfully by National Aeronautics and Space Administration to control fluid fuel in a weightless environment for the first time in 1963. It is composed of nanometer magnetic particles (usually Fe_3O_4) with a typical diameter of 10 nm, surfactant, and liquid-carrier. The nanometer magnetic particles, coated by the surfactant, are uniformly distributed in the liquid-carrier forming a stable colloid solution. The magnetic fluid will flow to and maintain at the place where the magnetic field is stronger, thus we can control the magnetic fluid by magnetic field.

The combination of magnetism and fluidity makes it possible for magnetic fluid to suspend stably an object whose density is greater than that of magnetic fluid, and this particular phenomenon was discovered by Rosensweig for the first time in 1966 [1, 2]. Later in the book titled "*ferrohydrodynamic*", Rosensweig gave a detailed description on the particular magnetic levitation force (self-suspension buoyancy) by means of magnetic fluid stress tensor [3]. Up to now, this property of magnetic fluid has been exploited in many innovative devices, such as dampers [4-6], sensors [7-11], actuators [12-14], bearings [15, 16], micromechanical system [17-19] and so on.

For the typical application of the self-levitation of permanent magnet in magnetic fluid, for example, magnetic fluid sensor [20, 21], damper [22, 23] or energy harvester [24] the diagram of which is shown in Fig. 1. The permanent magnet levitates itself in magnetic fluid contained in a cylindrical container under the magnetic field created by the permanent magnet itself. The permanent magnet is finely balanced in the container radially and damped by the magnetic fluid from radial and axial movements. With axial and radial acceleration (or vibration), the permanent magnet deviates from the center both in radial and axial direction. Axial accelerations tend to produce an axial movement (change of D as shown in Fig. 1) of the magnet which is resisted by the axial magnetic levitation force experienced by the magnet. Radial vibration will

*Corresponding author: Tel: +86 13810204816
Fax: +86-10-51684006, e-mail: dcli@bjtu.edu.cn, 16116356@bjtu.edu.cn

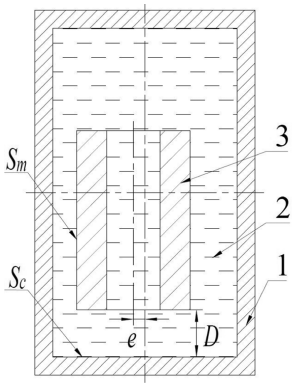

Fig. 1. The diagram of a ring magnet suspended in a container filled with magnetic fluid: 1-container, 2-magnetic fluid, 3-ring permanent magnet.

give the inertia mass a radial eccentricity (e as shown in Fig. 1).

Since the vast majority of applications utilize the movement of the magnet in axial direction, the axial magnetic levitation force, which determines the axial movement of the magnet is a key factor to design and manufacture magnetic fluid sensor (damper or energy harvester). But for the use of the magnetic fluid sensor in application, the radial eccentricity of the magnet is useless but inevitable. So, there is a necessity to figure out whether the radial eccentricity has an influence on the axial magnetic levitation force experienced by the magnet.

In the previous studies, for example, in [7, 25-29], the magnetic levitation force experienced by a cylindrical magnet in a cylindrical container filled with magnetic fluid was studied without considering the influence of the radial eccentricity on the axial magnetic levitation force. In [22], the radial magnetic levitation force acting on the cylindrical magnet was studied, but the relationship between radial eccentricity and axial magnetic levitation force was not discussed. The ring magnet has been used in magnetic fluid sensors and dampers as described in [9, 10] and [30], but so far, few articles have studied the magnetic levitation force experienced by a ring magnet self-suspended in magnetic fluid.

In this paper, the axial magnetic levitation force is studied by numerical calculation, magnetic field simulation, and experimental measurement without radial eccentricity at first. Then, the influence of the radial eccentricity of the ring magnet on axial magnetic levitation force is discussed.

2. Theoretical Analysis

2.1. Theoretical analysis of magnetic levitation force

According to [3], the equation of motion for magnetic fluid can be expressed as

$$\rho \frac{d\boldsymbol{v}}{dt} = -\nabla p^* + \mu_0 M \nabla H + \rho \boldsymbol{g} + \eta \nabla^2 \boldsymbol{v} \tag{1}$$

where ρ is the density of magnetic fluid, $\boldsymbol{v}$ is the velocity of magnetic fluid, p^* is the composite pressure in magnetic fluid, μ_0 is the permeability of vacuum, H is the magnitude of magnetic field intensity, M is the magnitude of magnetization of the magnetic fluid, $\boldsymbol{g}$ is the acceleration of gravity, and η is the first coefficient of viscosity of magnetic fluid.

When the ring magnet suspended in a container filled with magnetic fluid as shown in Fig. 1, the magnetic fluid is at rest with $\boldsymbol{v} = 0$, and equation (1) becomes

$$0 = -\nabla p^* + \mu_0 M \nabla H + \rho \boldsymbol{g} \tag{2}$$

Integrating equation (2) over the volume of magnetic fluid and ignoring the boundary effect which appears at the boundary of the magnetic fluid (S_m and S_c as shown in Fig. 1) caused by the different magnetic permeability between magnetic fluid and the magnet, as well as, between magnetic fluid and the container. we have

$$\int_{V_{mf}} (-\nabla p^* + \mu_0 M \nabla H + \rho \boldsymbol{g}) dV = 0 \tag{3}$$

where V_{mf} is the volume of magnetic fluid, and dV is the infinitesimal volume element.

According to [3], p^* can be expressed as

$$p^* = p + p_s + p_m \tag{4}$$

where p is the pressure in magnetic fluid in the absence of magnetic field, p_s is magnetostrictive pressure which can be negligible for an incompressible magnetic fluid, and p_m is the fluid-magnetic pressure in magnetic fluid which can be expressed as

$$p_m = \mu_0 \int_0^H M dH \tag{5}$$

According to divergence theorem, for p^*, we have

$$-\int_{V_{mf}} \nabla p^* dV = -\int_{V_{mf}} \nabla p dV - \int_{V_{mf}} \nabla p_m dV = \int_{S_m+S_c} p_m \boldsymbol{n} da + \int_{S_m+S_c} p \boldsymbol{n} da \tag{6}$$

where da is the infinitesimal area element, $\boldsymbol{n}$ is the unit vector normal to da pointing to magnetic fluid, S_m is the surface of the magnet, and S_c is the surface of the container as shown in Fig. 1.

By equation (6), we have

$$-\int_{V_{mf}} \nabla p dV = \int_{S_m+S_c} p \boldsymbol{n} da \tag{7}$$

and

$$-\int_{V_{mf}} \nabla p_m dV = \int_{S_m} p_m \boldsymbol{n} da + \int_{S_c} p_m \boldsymbol{n} da \tag{8}$$

The magnetic levitation force experienced by the magnet which is the also magnetic force of magnetic fluid on the magnet can be expressed as

$$\boldsymbol{F}_m = -\int_{V_{mf}} \nabla p_m dV - \int_{S_m} p_m \boldsymbol{n} da = \int_{S_c} p_m \boldsymbol{n} da \tag{9}$$

where $\boldsymbol{n}$ is the unit vector normal to da pointing to the magnetic fluid.

If the permeability of magnetic fluid χ is set to be a constant, equation (9) can be rewritten as

$$\boldsymbol{F}_m = \frac{1}{2}\oint_{S_c}\left(\mu_0 \int_0^H \chi H dH\right)\boldsymbol{n} da = \frac{1}{2}\mu_0 \chi \oint_{S_c} H^2 \boldsymbol{n} da \tag{10}$$

From equation (10), we can get the magnetic levitation force acting on the magnet as long as the magnetic field strength over S_c is clear.

2.2. Calculation of the magnetic field strength in magnetic fluid

For a ring magnet with axial uniform magnetization, we can build the physical model using Ampere molecular circulation [31, 32]. The molecular currents cancel out each other inside the ring magnet and over the two end surfaces of the ring magnet, and a net current will appear on the two side surfaces of the ring magnet with the same magnitude but opposite in direction.

For a magnet, we have [33]

$$\frac{|\boldsymbol{J}_0|}{\mu_0} = \frac{J_0}{\mu_0} = i_m \tag{11}$$

where $\boldsymbol{J}_0$ (or $\boldsymbol{B}_r$) is the remanence vector of the magnet, i_m is line current density along the shaft of the cylindrical volume (the current per unit length).

To calculate the magnetic field effectively, we establish a cylindrical coordinate system, as well as a cartesian coordinate system, as shown in Fig. 2. The origin of the coordinate is set in the center of one end of the magnet with Z-axis coincides with the axis of the ring magnet. $P(C, \delta, D)$ is a point outside the ring magnet expressed in cylindrical coordinates, r_i, r_o, and l_m are the inside radius, outer radius, and axial length of the ring magnet, respectively.

According to the superposition principle of the field, the magnetic induction intensity $\boldsymbol{B}$ at point P must be the vector sum of $\boldsymbol{B}_o$ (the magnetic induction intensity generated by the magnetizing current over the outer surface of the ring magnet) and $\boldsymbol{B}_i$ (the magnetic induction intensity created by the magnetizing current over the inner surface of the ring magnet).

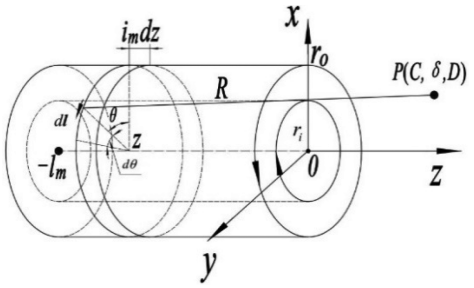

Fig. 2. The cylindrical coordinate and cartesian coordinate system.

The displacement vector from the current element $i_m$dzd$\boldsymbol{l}$ over the outer side surface of the ring magnet to the point $P(C, \delta, D)$ can be expressed as

$$\boldsymbol{R}_o = (C\cos\delta - r_o\cos\theta)\boldsymbol{e}_x + (C\sin\delta - r_o\sin\theta)\boldsymbol{e}_y + (D-z)\boldsymbol{e}_z \tag{12}$$

where $\boldsymbol{e}_x$, $\boldsymbol{e}_y$, and $\boldsymbol{e}_z$ are the unit vector of X-axis, Y-axis, and Z-axis in cartesian coordinate system, respectively.

The direction of the small current element can be written as

$$d\boldsymbol{l} = -r_o\sin\theta d\theta \boldsymbol{e}_x + r_o\cos\theta d\theta \boldsymbol{e}_y \tag{13}$$

Due to the symmetry of the magnetic induction intensity generated by the ring magnet, the magnitude of magnetic induction B must be the same in the place where the coordinate value C and D are the same in the cylindrical-coordinate system. With δ of $P(C, \delta, D)$ varying from 0 to 2π, B doesn't change in magnitude. At the point $P(C, 0, D)$, the magnitude of the displacement vector $\boldsymbol{R}_o$ can be given as

$$\begin{aligned} R_o &= \sqrt{(C - r_o\cos\theta)^2 + (r_o\sin\theta)^2 + (D-z)^2} \\ &= \sqrt{C^2 - 2r_oC\cos\theta + (D-z)^2 + r_o^2} \end{aligned} \tag{14}$$

According to Biot-Savart Law, $\boldsymbol{B}_o$ at the point $P(C, 0, D)$ can be given as

$$\begin{aligned} \boldsymbol{B}_o = &\frac{J_0}{4\pi}\int_{-l_m}^{0}\int_0^{2\pi}\frac{r_o(D-z)\cos\theta}{R_o^3}d\theta dz\boldsymbol{e}_x + \\ &\frac{J_0}{4\pi}\int_{-l_m}^{0}\int_0^{2\pi}\frac{r_o(D-z)\sin\theta}{R_o^3}d\theta dz\boldsymbol{e}_y + \\ &\frac{J_0}{4\pi}\int_{-l_m}^{0}\int_0^{2\pi}\frac{(r_o^2 - Cr_o\cos\theta)}{R_o^3}d\theta dz\boldsymbol{e}_z \\ = &B_{ox}\boldsymbol{e}_x + B_{oy}\boldsymbol{e}_y + B_{oz}\boldsymbol{e}_z \end{aligned} \tag{15}$$

where B_{ox}, B_{oy}, and B_{oz} are the components of the mag-

netic field intensity $\boldsymbol{B}_o$ at X, Y, and Z-axes in Descartes coordinate system, respectively.

Similarly, $\boldsymbol{B}_i$ be expressed as

$$\boldsymbol{B}_i = B_{ix}\boldsymbol{e}_x + B_{iy}\boldsymbol{e}_y + B_{iz}\boldsymbol{e}_z \tag{16}$$

Thus, we get the magnitude of magnetic field intensity generated by the ring magnet as

$$B = \sqrt{(B_{ox} - B_{ix})^2 + (B_{oy} - B_{iy})^2 + (B_{oz} - B_{iz})^2} \tag{17}$$

3. Numerical Calculation, Simulation, and Experiment

For the typical magnetic fluid inertia sensor, a cylindrical container is used as shown in Fig. 3. We will first do the calculation and simulation with the assumption that the axis of the ring magnet and the container are overlapped, and then the effect of radial eccentricity on axial magnetic levitation force will be discussed.

l_c = 45 mm and r_c = 15 mm are the length and radius of the cylindrical container, respectively. l_m = 15 mm, r_i = 3 mm and r_o = 7.5 mm, and the susceptibility of magnetic fluid used in calculation and simulation is χ = 0.36. D is the axial distance between the bottom of the container and magnet in range of 0-15 mm, when D = 15 mm, the ring magnet is in the center of the container. C is the radial distance from the point P to the axis of the container.

For the cylindrical container used in this paper, the inner surface S_c can be expressed as

$$S_c = S_{cb} + S_{cs} + S_{ct} \tag{18}$$

where S_{cb}, S_{cs} and S_{ct} are the bottom, side, and top surface of the cylindrical container, respectively. Due to the symmetry of the magnetic field, the integral of p_m over S_{cs} must be zero, and equation (10) can also be written as

$$\boldsymbol{F}_m = \frac{1}{2}\mu_0\chi\oint_{S_{cb}} H^2\boldsymbol{n}da + \frac{1}{2}\mu_0\chi\oint_{S_{ct}} H^2\boldsymbol{n}da \tag{19}$$

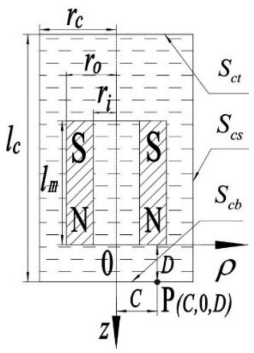

Fig. 3. A ring magnet suspended in a cylindrical container.

3.1. Numerical calculation

According to (15)-(17), we can get the magnitude of magnetic induction intensity B by MATLAB with just tens of lines of codes. The ring permanent magnet works on its demagnetization curve, the actual remanence is less than the theoretical one, and we set the actual remanence J_0 = 1.05T (The magnet is made of NdFeB, and the grade of the ring magnet is N35). Suppose that the region of the magnetic fluid is infinite with no flux refraction effect as shown in Fig. 4(a), and the magnitude of magnetic field intensity is

$$H = \frac{B(1+\chi)}{\mu_0(1+\chi)} = \frac{B}{\mu_0} \tag{20}$$

Let D remain the same for the time being with C varies within the range of 0-10 mm, we can get H over the plane whose axial distance is D from the bottom of the magnet (or H over S_{cb}). Then change the value of D, and the magnitude of magnetic field intensity is shown in Fig. 4(b). Based on the magnetic field described in Fig. 4(b), the numerical calculation results of axial magnetic levitation force are presented in Fig. 4(c).

3.2. Simlution

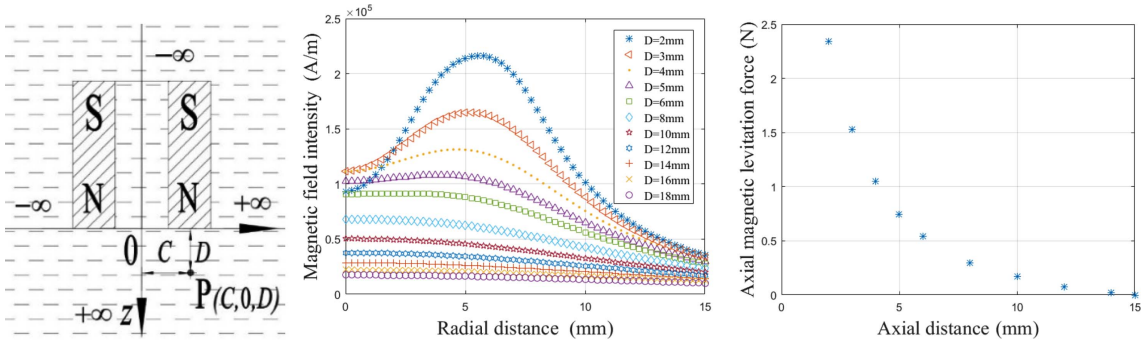

(a) (b) (c)

Fig. 4. (Color online) (a) Numerical calculation model of magnetic field. (b) The magnetic field over the bottom of the container got by numerical calculation. (c) Numerical calculation results of the axial magnetic levitation force.

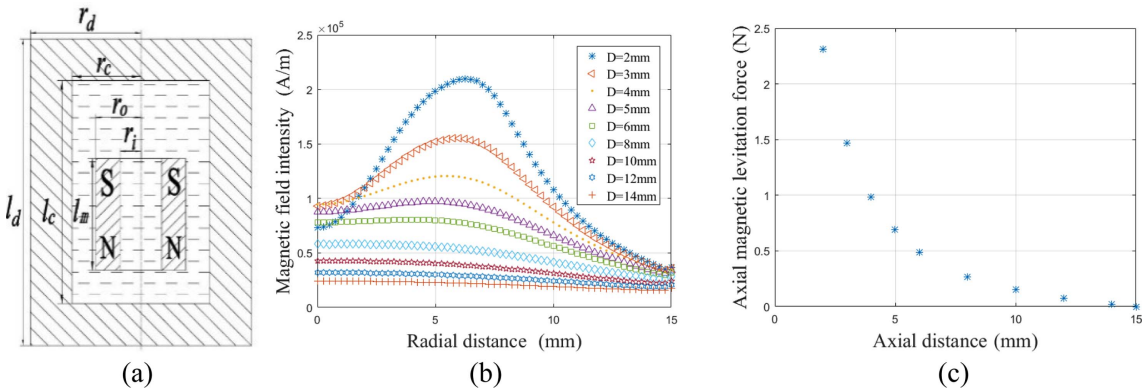

Fig. 5. (Color online) (a) The physical model of magnetic field simulation; (b) The magnetic field over the bottom of the container got by magnetic field simulation; (c) The simulation results of axial magnetic levitation force.

In addition to numerical calculation, the magnetic field intensity over S_{cb} and S_{ct} can also be got by magnetic field simulation using ANSYS. The remanence of the cylindrical magnet is B_r = 1.21T with the coercivity H_c = 963000 A/m. The physical model of magnetic field simulation is presented in Fig. 5(a), l_d is the length of the cylindrical computational domain whose magnitude is 180 mm, and r_d is the radius of the computational domain, the magnitude of which is 60 mm. The boundary condition of the magnetic field simulation is that the magnetic line is parallel to the boundary of the computational domain. The magnetic field intensity obbtained by simulation is shown in Fig. 5(b) and the simulation results of axial magnetic levitation force are shown in Fig. 5(c).

3.3. Experiment

To measure the axial magnetic levitation force experimentally, a thin, nonmagnetic aluminum rod is attached to the top end surface of the magnet. The experimental schematic diagram is shown in Fig. 6(a), the digital Vernier caliper connecting with the dynamometer is installed on the vertical guide screw, which can move up and down when the handle is rotating. The ring magnet is connected with the dynamometer by the thin aluminum rod. The digital Vernier caliper can detect the displacement of the magnet in vertical direction while the dynamometer can measure the axial magnetic levitation force experienced by the ring magnet. The density of the magnetic fluid is 1333 Kg/m^3. The ring magnet has immersed in magnetic fluid for about 3 days before measurement, and the experimental results are shown in Fig. 6(b).

4. Results and Discussion

The numerical calculation, simulation and experimental results are presented in Fig. 7, it is obvious that the numerical calculation, simulation and experimental results

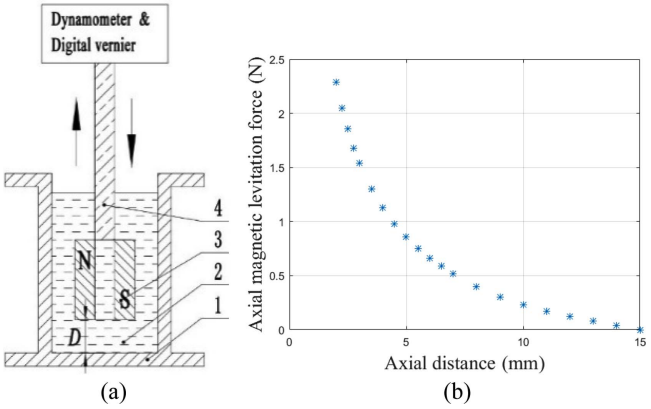

Fig. 6. (Color online) (a) Experimental schematic diagram: 1-container, 2-magnetic fluid, 3-ring magnet, 4-nonmagnetic aluminum rod; (b) The experimental results of axial magnetic levitation force.

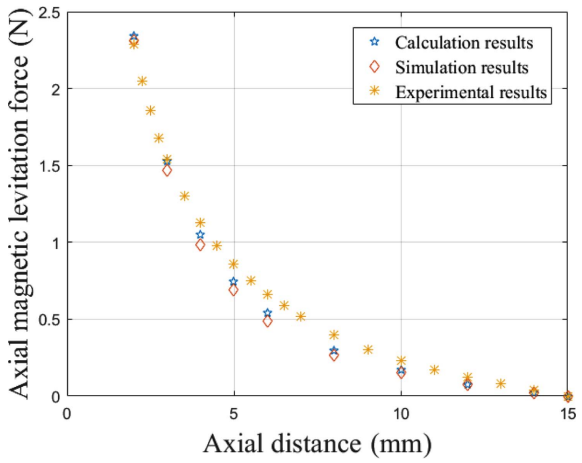

Fig. 7. (Color online) The comparison of numerical calculation, simulation, and experimental results.

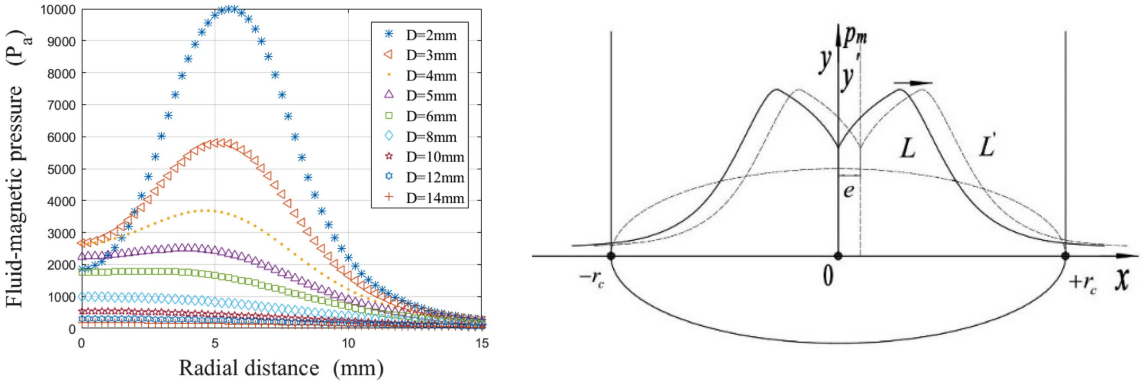

(a) (b)

Fig. 8. (Color online) (a) The distribution of fluid-magnetic pressure over the bottom of the container; (b) The set coordinate to study the influence of radial eccentricity on axial levitation force.

are in agreement with each other. The axial magnetic levitation force will grow rapidly when the ring magnet moves down.

Now we will discuss the influence of radial eccentricity on the axial magnetic levitation force. According to the distribution of H presented in Fig. 4(b), we can draw the distribution of p_m over S_{cb} as shown in Fig. 8(a). We can see from Fig. 8(a) that when the ring magnet gets close to S_{cb}, p_m over S_{ct} can be ignored. Therefore, equation (19) can also be written as

$$\boldsymbol{F}_m \approx \frac{1}{2}\mu_0\chi \oint_{S_{cb}} H^2 \boldsymbol{n} da \tag{21}$$

To study the effect of radial eccentricity on the axial levitation force, we set a coordinate system as shown in Fig. 8(b). The origin of coordinate is set at the center of S_{cb}, and X-axis lies on S_{cb} with Y-axis normal to S_{cb}. Y-axis gives the magnitude of p_m and X-axis gives the radial distance from a point to the origin of the coordinate.

When the symmetry axis of the ring magnet coincides with that of the container, the magnetic field in magnetic fluid is symmetry about the Y-axis, and also p_m (the solid line denoted by L as presented in Fig. 8(b)) is symmetry about the Y-axis. If we rotate the solid line L around the Y-axis for 180 degrees, we get a surface which we shall denote by V_L. The volume enclosed by the surface S_L, S_{cs}, and S_{cb}, let's denote it by V_L, equals the magnitude of the axial levitation force acting on the ring magnet.

When the ring magnet deviates from the axis of the container in radial direction, for example, a distance e as shown in Fig. 8(b), p_m over S_{cb} will change with the change of the eccentricity e, and also the axial levitation force acting on the magnet. If we ignore the influence of magnetic field refraction effect, the magnetic field generated by the ring magnet will be symmetry about ring magnet's symmetry axis, as the dotted line L' presented in Fig. 8(b). we rotate the dotted line L' around the symmetry axis of the ring magnet, y', for 180 degrees, and get a surface which we shall denote by S_L . And the volume enclosed by the surface S_L' , S_{cs}, and S_{cb}, let's denote it by V_L' , equals the magnitude of the axial levitation force in this case.

According to Fig. 8(b), the magnitude of the enclosed volume should be the maximum when the symmetry axis of the ring magnet coincides with that of the container, and $\Delta V_L = V_L' - V_L < 0$. The magnitude of the enclosed volume, which equals the magnitude of the axial magnetic levitation force experienced by the ring magnet will decrease with the emerging of any given radial eccentricity e. It is

$$\Delta F_m = F_m' - F_m < 0 \tag{22}$$

With the increase of the radial eccentricity e, the magnitude of the axial magnetic levitation force F_m will continue to decrease. In this paper, according to the distribution of p_m presented in Fig. 8(a), ΔF_m will be small compared to the magnitude of F_m. To verify this, we measure F_m with the same D but different e experimentally. When D = 2 mm with F_m = 2.29N, the ΔF_m corresponding to different eccentricity e is given in

Table 1. The relationship between ΔF_m and e.

e (mm)	1	2	3	4
ΔF_m (N)	0	–0.01	–0.03	–0.04

Table 2. The relationship between ΔF_m and e.

D (mm)	2	4	6
ΔF_m (N)	–0.04	–0.02	0

Table 1.

When D gets smaller, p_m over S_{cb} gets larger, and for the same e, the difference between V_L' and V_L becomes larger which indicates that the magnitude of ΔF_m will increase with the decrease of D for the same e. To verify this, we measure F_m with the same eccentricity e but different D experimentally. When e = 4 mm, the ΔF_m corresponding to different distance D is given in Table 2.

5. Conclusion

In this paper, the axial magnetic levitation force experienced by a ring magnet suspended in magnetic fluid is studied and attention is paid to the influence of the ring magnet's radial eccentricity on the axial magnetic levitation force. We obtain the magnetic field in magnetic fluid by numerical calculation and magnetic field simulation based on which the axial magnetic levitation force is calculated. Besides, we measure the magnetic levitation force experimentally, and the experimental results, numerical calculation results, and simulation results agree well with each other. Both theoretical analysis and experimental results show that the ring magnet will experience a maximum axial magnetic levitation force without radial eccentricity, the axial magnetic levitation force will decrease with the emerging of radial eccentricity. With the increase of radial eccentricity and the decrease of the distance between the bottom of the ring magnet and container, the axial magnetic levitation force will continue to decrease, but the magnitude of the change is negligible compared to that of the axial magnetic levitation force. In the research following this paper, we can fill the hole of ring magnet with something, for example, a ferromagnetic material, through which we can expect a change of magnetic levitation force acting on the ring magnet.

Acknowledgement

This work was supported by "the Fundamenal Research Funds for the Central Universities" (Grant No. 2018YJS145) and "National Defense Science and Technology Innovation Special Zone Project" (Grant No. 18-163-21-TS-001-007-01).

References

[1] R. E. Rosensweig, AIAA J. **4**, 10 (1966).
[2] R E Rosensweig, Nature **210**, 5036 (1966).
[3] R. E. Rosensweig, Ferrohydrodynamics (Cambridge University, New York, 1997) pp 33-73.
[4] Chuan Huang, Jie Yao, Tianqi Zhang, Yibiao Chen, Huawei Jiang, and Decai Li, J. Magn. **22**, 1 (2017).
[5] X. R. Yang, Q. X. Yang, W. R. Yang, B. Guo, and L. F. Chen, IEEE Trans. Appl. Supercond. **28**, 3 (2018).
[6] Jinghui Peng, Songjing Li, and Hasiaoqier Han, Appl. Phys. Lett. **104**, 17 (2014).
[7] Jun Yu, Xinzhi He, Decai Li, and Wenyi Li, IEEE Sens. J. **18**, 6 (2018).
[8] R. Olaru and D. D. Dragoi, Sensors and Actuators a-Physical **120**, 2 (2005).
[9] D. Y. Lagutkina and M. S. Saikin, J. Magn. Magn. Mater. **431**, (2017). DOI: 10.1016/j.jmmm.2016.11.040
[10] Jie Yao, Yibiao Chen, Zhenkun Li, Tianqi Zhang, and Decai Li, Smart Materials and Structures **25**, 9 (2016).
[11] L. P. Qian, D. C. Li, and J. Yu, IEEE Sens. J. **16**, 23 (2016).
[12] R. Olaru, A. Arcire, C. Petrescu, and M. M. Mihai, Ieej Trans. Elect. Electron. Eng. **12**, 1 (2017).
[13] Shuai Wu, Chunfang Li, Xiangyu Zhao, and Zongxia Jiao, Appl. Phys. Lett. **111**, 21 (2017).
[14] Babak Assadsangabi, Min Hian Tee, and Kenichi Takahata, J. Microelectromechanical Systems **23**, 5 (2014).
[15] S. G. E. Lampaert, J. W. Spronck, and R. A. J. van Ostayen, Proceedings of the Institution of Mechanical Engineers Part J-Journal of Engineering Tribology **232**, 1 (2018).
[16] Nimeshchandra S. Patel, Dipak Vakharia, and Gunamani Deheri, Industrial Lubrication and Tribology **69**, 5 (2017).
[17] Sayed Mohammad Hashem Jayhooni, Babak Assadsangabi, and Kenichi Takahata, Sensors and Actuators A: Physical **269**, (2018). DOI: 10.1016/j.sna.2017.11.020
[18] Shuai Wu, P. C. K. Luk, Chunfang Li, Xiangyu Zhao, Zongxia Jiao, and Yaoxing Shang, Applied Energy **197**, (2017). DOI: 10.1016/j.apenergy.2017.04.006
[19] Shuai Wu, P. C. K. Luk, Chunfang Li, Xiangyu Zhao, and Zongxia Jiao, IEEE Trans. Magn. **53**, 9 (2017).
[20] L. P. Qian and D. C. Li, Journal of Sensors (2014).
[21] Leping Qian, Decai Li, and Jun Yu, IEEE Sens. J. **15**, 12 (2015).
[22] W. M. Yang, P. K. Wang, R. C. Hao, and B. H. Ma, J. Magn. Magn. Mater. **426**, (2017). DOI: 10.1016/j.jmmm.2016.11.099
[23] Wenming Yang, Decai Li, Xinzhi He, and Qiang Li, Int. J. Appl. Electromagnetics Mech. **40**, 1 (2012).
[24] Y. Wang, Q. Zhang, L. Zhao, Y. Tang, A. Shkel, and E. S. Kim, Appl. Phys. Lett. **109**, 20 (2016).
[25] Jun Yu, Jiawei Chen, and Decai Li, J. Magn. Magn. Mater. **469**, (2019). DOI: 10.1016/j.jmmm.2018.08.080
[26] Jun Yu, Du Hao, and Decai Li, J. Phys. D-Appl. Phys. **51**, 1 (2018).
[27] Jun Yu, Xinzhi He, Decai Li, and Wenyi Li, Phys. Fluids **30**, 9 (2018).
[28] Wenming Yang, J. Vib. Control. **23**, 14 (2017).
[29] Xinzhi He Jun Yu, Decai Li and Rongkun Dai, Journal of Beijing Jiaotong University **42**, 4 (2018).
[30] S. Sudo and A. Nakagawa, Int. J. Mod. Phys. B **19**, 7

(2005).
[31] C. Q. Zhang, P. Zhao, F. Gu, J. Xie, N. Xia, Y. He, and J. Z. Fu, Anal. Chem. **90**, 15 (2018).
[32] C. Akyel, S. I. Babic, and M. M. Mahmoudi, Progress in Electromagnetics Research-Pier **91**, (2009). DOI: 10.2528/PIER09021907
[33] P. C. Xia, Permanent magnetic mechanism (Beijing University of Technology Press, Beijing, 2000) p 4.